EVS29 Symposium
Montréal, Québec, Canada, June 19-22, 2016

Degradation mechanism detection for NMC batteries based on Incremental Capacity curves

M. Berecibar [1,2], M. Dubarry [3], N. Omar [2], I. Villarreal [1], J. Van Mierlo [2]

[1] *IK4-Ikerlan, Energy Business Unit, Technology Park of Alava, 01510, Minano, Spain*

[2] *Vrije Universiteit Brussel, MOBI Research Group, Pleinlaan 2, 1050 Brussels*

[3] *Hawaii Natural Energy Institute, SOEST, University of Hawaii at Manoa, 1680 East-West Road, POST 109, Honolulu, Hl 96822, USA*

(mberecibar@ikerlan.es; mberecib@vub.ac.be)

Summary

Path dependence degradation detection is getting lot of attention due to high demand of long lasting batteries for applications with sporadic usage such as electric vehicles. In this regard, this work presents a study of the degradation mechanism of NMC/Graphite cells cycled under different depth of discharges. Analysis will be based on the study of incremental capacity curves. The trends observed on experimental curves will be compared to simulations in order to exemplify the differences and highlight the path dependence of the degradation.

Keywords: Prediction, Nickel Manganese Cobalt Oxide Battery, Battery Management System, State of Health

Introduction

The requirements and demands that batteries have to meet are constantly increasing. Therefore, effective control and management is crucial for ensuring a safe use of the battery while maintaining the best possible performance. Despite the fact that the diagnosis and prognosis of the State of Health (SoH) is absolutely essential in practical applications, they are not yet effectively implemented in Battery Management Systems (BMS). The main issue hampering the ability of BMSs to accurately track the SoH is the evolution of the voltage response of the cells with aging coupled with the path dependence of the degradation. The latter is a premier issue because it prevents the BMS to use preset look-up tables for SoC recalibration upon aging.

Path dependence is challenging to take in consideration because of the numerous degradation mechanisms that can occur throughout the life of a cell. It was shown that a multitude of parameters play a key role in degrading a Li-ion cell: depths of discharge (DoD), states of charge, applied currents, temperatures, calendar aging conditions, pulses…[1–4] In real life those parameters cannot be controlled and it is impractical to replicate all of them in a laboratory setting.

Operando degradation mechanisms detection is of huge importance in order to try to detect and quantify ageing in a cell. It will be a key feature as to predict degradation and SoH of a battery cell and thus on the ability of a BMS to handle path dependence. One attractive way to address this issue is to analyze battery degradation using differential voltage techniques. These techniques have been used by many researchers [5–8] in order to reveal battery degradation mechanisms and they were shown successful in quantifying the

individual components of every degradation mechanism: the extent of Loss of lithium inventory (LLI), loss of active material (LAM) and kinetic changes.

In this work, we will use incremental capacity (IC) as the differential voltage technique. Additionally, we will be using the *'alawa* toolbox developed by M. Dubarry *et al.* [5,9–11] in order to study the impact of each individual component of the degradation. The main purpose of the toolbox is the intricate study of the degradation mechanisms by emulation of different scenarios.

In this regard, this study presents an extensive research of the degradation mechanism of NMC/Graphite cells cycled at different DoD based on the study of IC curves. From the simulations and the tested cells, different features of interest have been observed and selected [12], highlighting path dependence.

2- Experimental

2.1 Cycling

Three high power 40Ah Li-ion cells containing Graphite (G) based anode and $LiNi_{1-x-y}Mn_yCo_xO_2$ (NMC) based cathode have been used for this work. Cells were cycled at different DoDs, Cell A was cycled at 80% DoD, Cell B at 60% and Cell C at 30% with the charging protocol being the same. The ageing tests were performed in a temperature controlled environment at 25°C (ClimaTemperatur-System, CTS/T-40/200/Li and CTS/T-40/600/Li models, and Prebatem Selecta 80 and 150 L chambers with Peltier effect). Experiments were carried out using DIGATRON MCT (Multiple Cell Tester, MCT 100- 06-10 ME and MCT 50-06-24 ME models) with BTS-600 battery data acquisition software. The cells were tested from the beginning of life (BoL) until the EoL (20% capacity loss, if reached).

Cycling was interrupted every 300 full equivalent cycles to perform reference performance tests (RPT). In this RPT, two tests were carried on the cells:

- Capacity test: charge and discharge cycles (at current-constant voltage, CC-CV, and CC modes, respectively) at nominal conditions specified by cell manufacturer (1C-rate current and 25 ºC temperature). Three full charge-discharge cycles were performed in order to assess both reversible and irreversible capacity losses and check the repeatability of the results.
- Cell full charge/discharge test: Prior to the discharge of the cells are fully charged in CC-CV mode at 1C. Discharge were performed at a C/5 rate. This Crate was chosen as it was the fastest one that enabled observing the voltage plateaus in view of implementation in real application where low rate cycling is impracticle. Galvanostatic voltage profiles were used for examining electrode phase changes and understanding degradation phenomena.

The SoH was calculated from the capacity test according to equation (1) were Q is the capacity in Ah (1).

$$SoH = \frac{Q_{Aged\ Battery}}{Q_{Fresh\ Battery}}\ x\ 100\% \tag{1}$$

2.2 Incremental capacity curves

The operation mode of lithium ion batteries is based on the intercalation and deintercalation of lithium-ions between the anode and the cathode. The difference in the lithium electrochemical potential of the electrodes defines the potential of the cell. Thus, in order to estimate the state of the battery, a key parameter is the cell voltage. This parameter depicts electrochemical reactions and their evolution [5]. In other words, the ability to analyse the cell voltage is the key to understand cell behaviour and degradation.

The variations on V vs. Q curves are usually pretty minute and hard to quantify. In order to ease the analysis, derivative methods, differential voltage and incremental capacity, could be used. For this work, as well as for the previous work regarding SoH estimation, incremental capacity technique is used. For this technique, the relationship between the two electrodes can be written as [7]:

$$\left(\frac{dQ}{dV}\right)_{cell} = \frac{1}{(dV/dQ)_{cathode} - (dV/dQ)_{anode}} \tag{2}$$

IC curves have already been used for ageing and degradation mechanisms detection in different battery technologies: LFP cells [5,13,14], LTO batteries [15], LCO [16] and NMC [8,17]. They have been studied also for SoH estimation, like in NMC cells [18–20], LFP [21–23] and also composites NMC+LMO [23] cells.

2.3 Alawa Toolbox

Emulation of IC curves were performed using the '*alawa* toolbox developed by M. Dubarry *et al.* [9,11,24]. The toolbox enables simulation of a wide array of degradation scenarios with different anode and cathode materials, composite or not, and operating conditions, etc. Its main advantage is to give the possibility to mix and match all the possible degradations mechanisms in order to obtain the best fitting solution.

In this work, the exact replicate of the anode and cathode were not available. The toolbox was then calibrated on a standard G//NMC cell and used to visualize the trends of voltage changes induced by individual degradation modes.

In order to emulate the cell behaviour in the *'alawa* toolbox, two parameters are necessary: the loading ratio between the negative and the positive electrode (LR) and the initial irreversible capacity loss of the negative electrode that compensates the SEI formation (OFS). These two parameters can typically be obtained from a discharge curve at C/25 at the beginning of life (BOL) [5]. In this study, the C/25 discharge at the beginning of life was not performed and therefore the LR and OFS were estimated from the initial C/2 discharge. The best fit that could be obtained were LR = 1.15 and OFS= -5.

3- Results

3.1 Cycling

The cells have been tested at 25°C at different depth of discharge levels (DoD). Cell A was cycled at 80% DoD, Cell B at 60% and Cell C at 30%. Cell A reached nearly an EoL state coming up to 82% capacity, cell B reached a 95% and cell C a 90% capacity. Cell B and cell C were not cycled to EoL because of time constraints. The cells degradation can be compared at three strategic points, BoL,95% SoH and 90% SoH (cells A and C only). The normalized capacity evolution of each cell can be seen at the left side of figure 1, the evolution of the IC curves obtained from the tested cells in terms of ageing are presented in the right side.

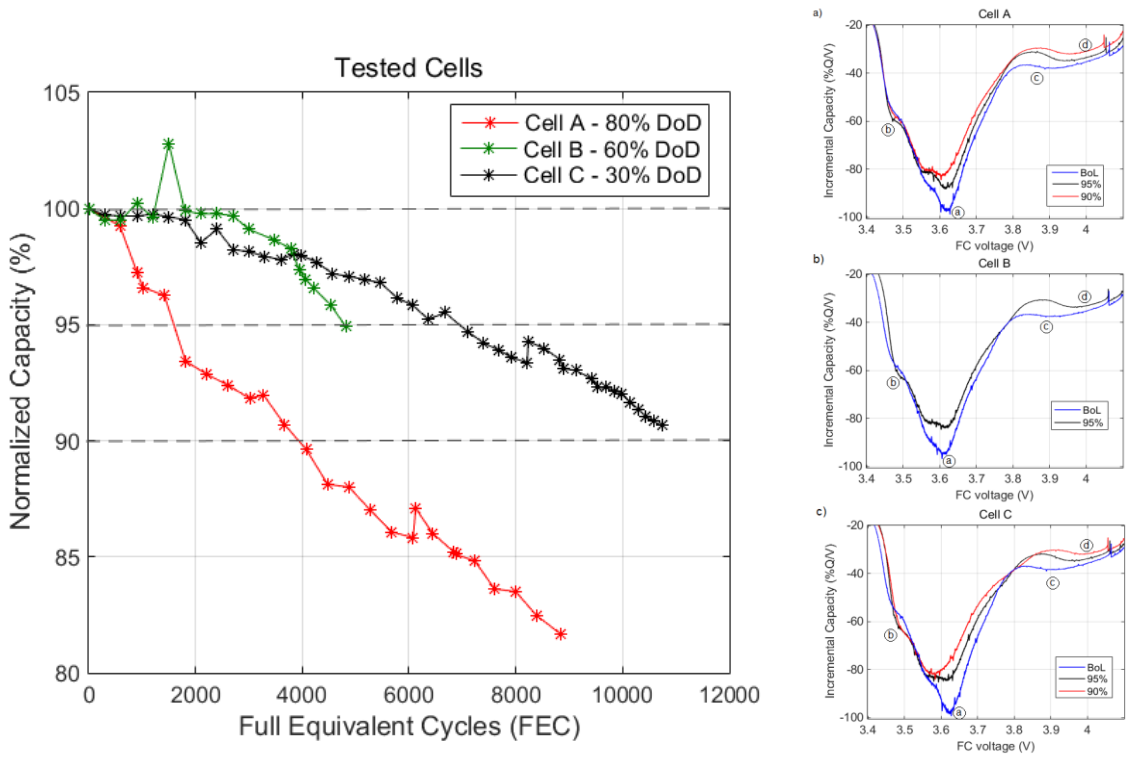

Figure 1: Capacity evolution of the tested cells on the left side, and evolution of IC curves obtained from the tested cells in terms of ageing on the right side.

In order to analyse ageing of the cells, the evolution of the IC curves with 5% increment in capacity loss are going to be studied. A clear evolution of the curves can be detected as the cells degrade and this evolution can be described from the changes of 4 main characteristics of the IC curves : two peaks (a) and (b) and two electrochemical features, an arch shape (c) and the intensity at 4V (d). The 2 peaks have their initial maximum of intensity at 3.6V (a) and 3.5V (b), respectively and this maximum of intensity seems to decrease and shift towards lower potentials with aging. The arch (c) appears to shift from 3.75 to 3.85V. The IC intensity at 4V, feature (d), seems to decrease with aging.

3.2 Simulated curves

The main objective of this work is to determine and detect the degradation mechanisms that are occurring in the cells. In order to identity their individual impact on cell performance, simulations from the BoL state until a 90% SoH have been performed using the *'alawa* toolbox. In this work we will focus only on thermodynamic changes and thus the kinetic factors will not be considered. As a result, 3 degradation mechanisms were studied in this work: Loss of Lithium Inventory (LLI), and the Loss of Active Material (LAM) on both electrodes at a delithiated state (the lithiated state is equivalent to the delithiated state plus some LLI). For sake of simpification, LAM_{dePE} and LAM_{deNE} will be referred as LAM_{PE} and LAM_{NE} in the rest of this work. Figure 3 shows the resulting IC curves obtained from the *'alawa* toolbox for a G//NMC cell with LR = 1.15 and OFS = -5 and a discharge rate of C/5.

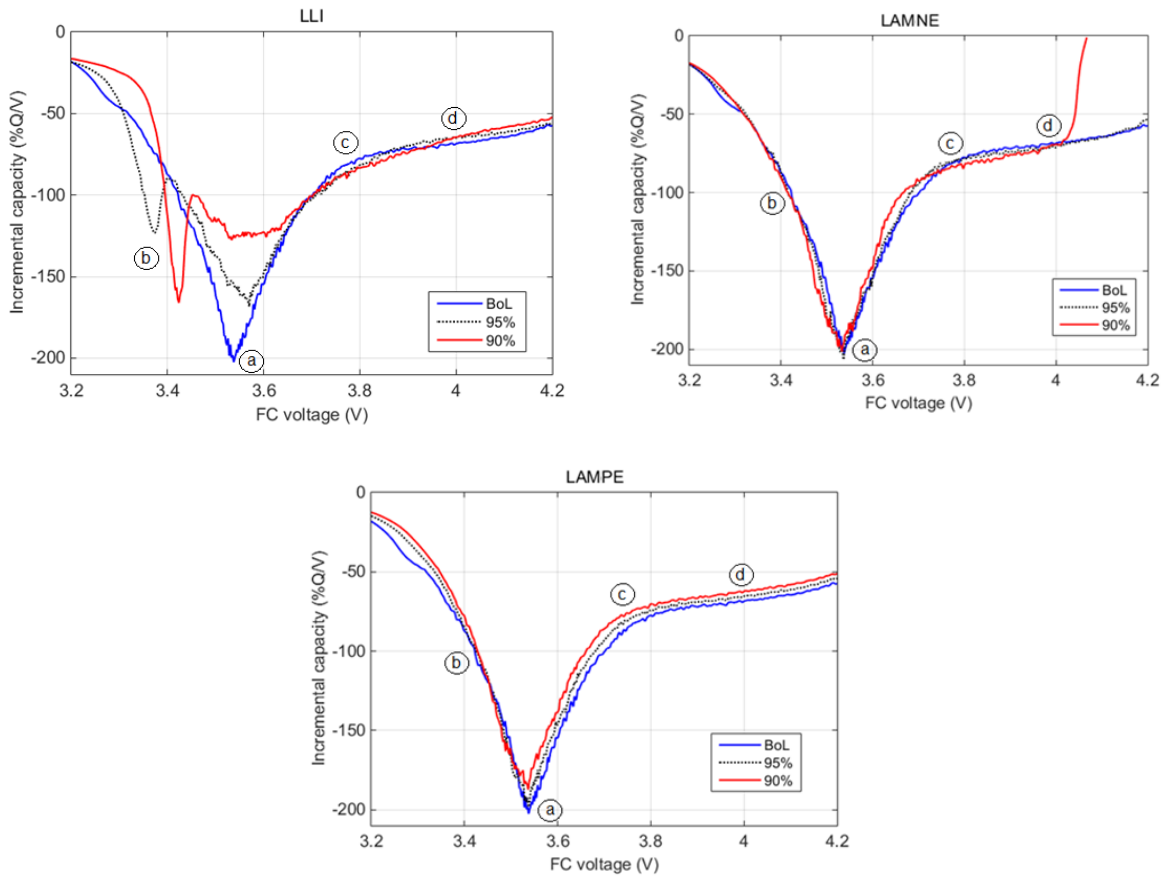

Figure 2: IC curves obtained from the *'alawa* toolbox for a G//NMC cell with LR = 1.15 and OFS = -5 and a discharge rate of C/5. (1) LLI, (2) LAM_{NE} and (3) LAM_{PE}.

The 4 main characteristics observed on the experimental data, (a), (b), (c) and (d) can be tracked for every individual degradation mode. As a result, the impact of the degradation modes on the selected features can be deciphered:

Starting with feature (a), which can be delimited as the most defined peak at approximately 3.6V. It can be detected that for both LAM scenarios the peak doesn't change significantly and only a slight intensity

increase can be observed for LAM_{PE}. In case of LLI (figure 2, case 1), the peak undoubtedly changes in both intensity, shape and position as it becomes less intense, broader and starts at higher voltages.

Something similar happens with feature (b) and the peak detected at 3.5 V. It can be easily recognized that in LAM_{NE} (figure 2, case 2) and LAM_{PE} (figure 2, case 3) this peak is not visible whereas, on the contrary, a new peak is appearing around 3.4 V when LLI is occurring (figure 2, case 1). This peak appears around 3.37V initially then moves towards higher voltages (3.42V) with further degradation. The intensity of the peak also changes, reaching higher intensity as the cell degrades.

The third detected feature refers to the arch, feature (c). This arch shape is not easily detected in any of the case of figure 2. In order to check the arch in the simulation curves, the data obtained for the discussion part is obtained from simulations at lower rates (not shown), in which the arch can be detected. The arch positon will be defined as the lowest intensity between 3.7 and 3.9 V.

The last characteristic to take into consideration is the incremental capacity intensity at 4V. In case of LLI (figure 2, case 1), the incremental capacity intensities do not change much with aging at 4V. The same can be observed with LAM_{NE} (figure 2, case 2). In case of LAM_{PE} (figure 2, case 3) the curves clearly reach progressively lower incremental capacity values upon degradation.

4- Discussion

4.1 Features of Interests

The evolution of the features of interests was studied in order to detect the degradation mechanisms in the cells. The detection was based on the study of the path that each feature follows upon aging. The comparison of the cells at similar SoHs (BoL, 95% SoH and 90% SoH) is presented in figure 3.

The first figure on the left shows the BoL IC curves of the 3 tested cells. Overall the cells presented similar features which suggests that the cells were at a similar SoH at the beginning of the experiment. It has to be noted that Cell B presented a slightly lower intensity for feature (a), the other 3 feature stayed nearly identical.

The second figure presents the IC signature of the 3 cells at 95% SoH. The intensity of feature (a) decreased for all the cells, by 14% for cells B & C and by 9% for cell A. The intensity of feature (b) increased with aging. Again, cells B and C presented a similar evolution of 3%. Cell A presented an increase of 0.5%. The voltage of feature (b) presented a shift to lower voltages. Cell A turned 10mV to a lower voltage position, on the contrary cells B and C shifted slightly less, moving 1mV and 6mV respectively. Feature (c) focuses on the arch shape between 3.7 and 3.9V. The arch intensity lowered by 6% with aging and shifted to higher voltages. The voltage shift was different for all cells, 21mV for cell A, 31 mV for cell B, and 54 mV for cell C. Finally, the intensity of feature (d) decreased by 2.5% for all the cells.

Lastly, in the figure showing a 90% SoH only cell A and C were available. The intensity of feature (a) decreased further for all the cells, by 4% for cell A and by 1.2% for cell C. The intensity of feature (b) kept increasing with aging, 1% for Cell C and 1.4% for Cell A. The voltage of feature (b) also shifted to higher voltages. Cells A shifted by 7mV and cell C by 4mV. Feature (c) intensity decreased by 1-2% for both cells. In terms of voltage, cell A shifted again towards higher voltages by 21 mV and cell C by 47 mV. Finally, the intensity of feature (d) decreased for all the cells, by 3% for cell A and 2% for cell C.

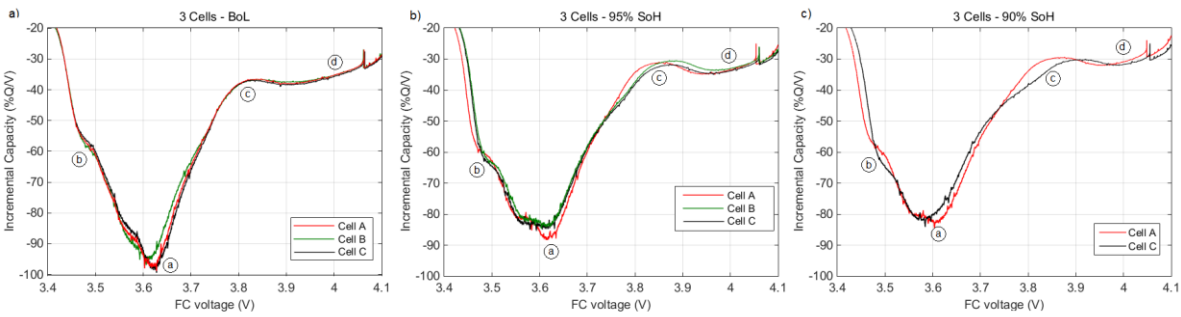

Figure 3: IC curves at different SoH for the three tested cells a) BOL, b) 95% SoH and c) 90% SoH.

Different simulations were performed by the use of the *'alawa* tool. The degradation mechanisms LLI, LAM_{NE} and LAM_{PE} were studied from a BoL state until a 90% SoH, checking the simulations every 1% SoH. Also all the different possible scenarios between the studied degradation mechanisms were considered: LLI+LAM_{PE}, LLI+LAM_{NE}, LAM_{PE}+LAM_{NE} and LLI+LAM_{PE}+LAM_{NE}. As a result, 7 degradation scenarios were investigated.

In the next section, the evolution of the features from the simulations are compared to the experimental ones.

Feature (a)

The peak at 3.6 V is the main feature towards degradation mechanism detection. As already detected and in order to have a careful study of it, two main properties will be analysed as the cell degrades: intensity and position.

- Intensity

  The intensity of the peak at 3.6V is decreasing with aging. This trend can be compared with the simulations in order to gain insight on possible degradation scenarios in figure 4-a. The tested three cells have a very similar performance. Since the simulations were performed on a reference cell and not the exact replicate of the tested cells, we'll focus more on the exclusion of scenarios rather than an exact fit of the variations. The 3 tested cell stay at the middle of the graph between 100 and 120% of the initial peak intensity. As a result, three scenarios seems incompatible: LLI, LLI+LAM_{NE} and LAM_{NE}. The first two are excluded because they predict a larger peak intensity increase, and for third one, because it predicts a decrease of the intensity.

- Voltage

  Figure 4-b presents the evolution of the position of the peak upon aging for the experimental data as well as different degradation scenarios. According to this figure, cells A and C behave in a different way than of the simulations with a more marked shift towards higher voltage. This is likely induced by the differences between the reference cell and the actual cell. In any case, scenarios predicting an increase of the voltage, LLI and LLI+LAM_{NE}, appear incompatible.

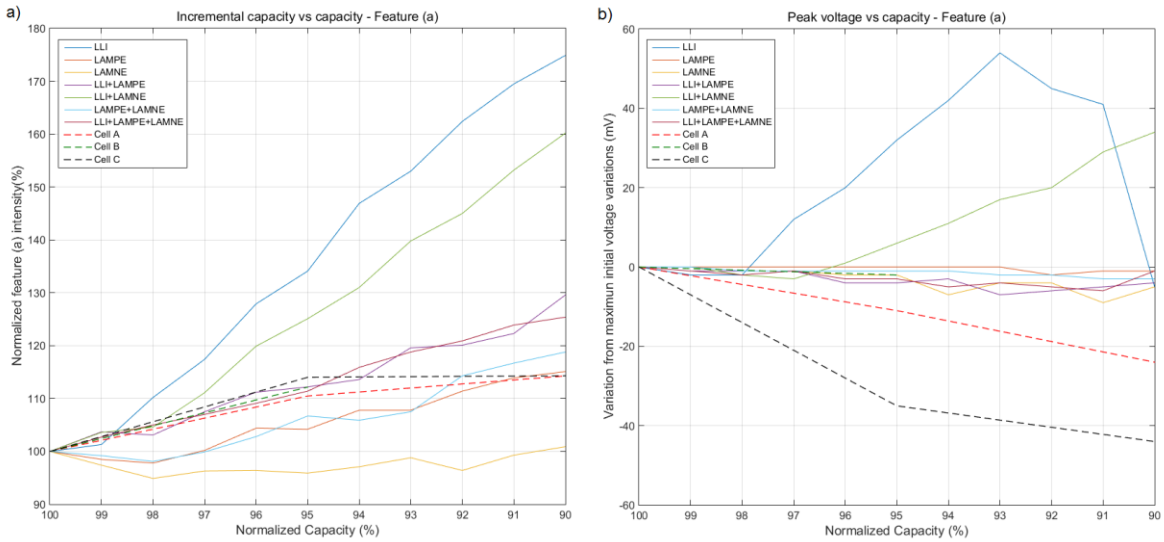

Figure 4: Normalize intensity and peak voltage evolution for feature (a).

4.1.1 Feature (b) peak

The second feature to take into consideration is the appearance of a small peak at 3.5V. Both characteristics, voltage and incremental intensity values will be taken into consideration.

- Intensity

  The peak at 3.5V of the tested cells reaches higher incremental capacity values with aging. The tested three cells have a very similar performance. According to the different simulations, LLI and LLI+LAM_{NE} scenarios seems incompatible.

- Voltage

Figure 5-b presents the evolution of the position of the peak upon aging for the experimental data as well as different degradation scenarios. It has to be noted that Cell B and Cell C overlaps. In the same way as in the intensity, the incompatible scenarios are pure LLI and LLI+LAM_{NE}.

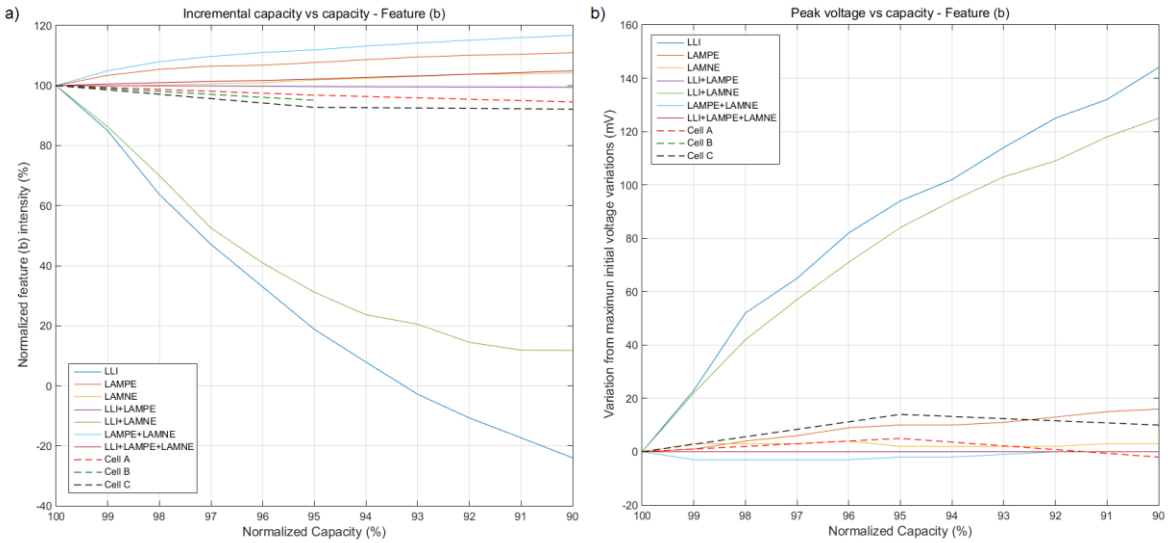

Figure 5: Normalize intensity and peak voltage evolution for feature (b).

4.1.2 Feature (c)

From the analysis of the changes of arch positon on the tested cells, the arch shifts towards higher voltages and that its intensity is decreasing.

- Intensity

Figure 6-a compares the variations of arch position for both the experimental data and the simulations. According to this comparison, the cells behave very similarly and the less likely scenarios to explain the variations are: LAM_{NE}, LLI and LAM_{PE} as they predict a decrease of the intensity.

- Voltage

According to the measured evolution of the arch voltage, it can be said that cells B and C share the same trend and cell A behaves differently. Cell A arch voltage reached lower values compared to the other two cells. Looking at the different scenarios, pure LLI scenario is unlikely due to the higher predicted values. LAM_{NE} and LAM_{PE}+LAM_{NE} scenarios also seems incompatible due to the low predicted voltage values.

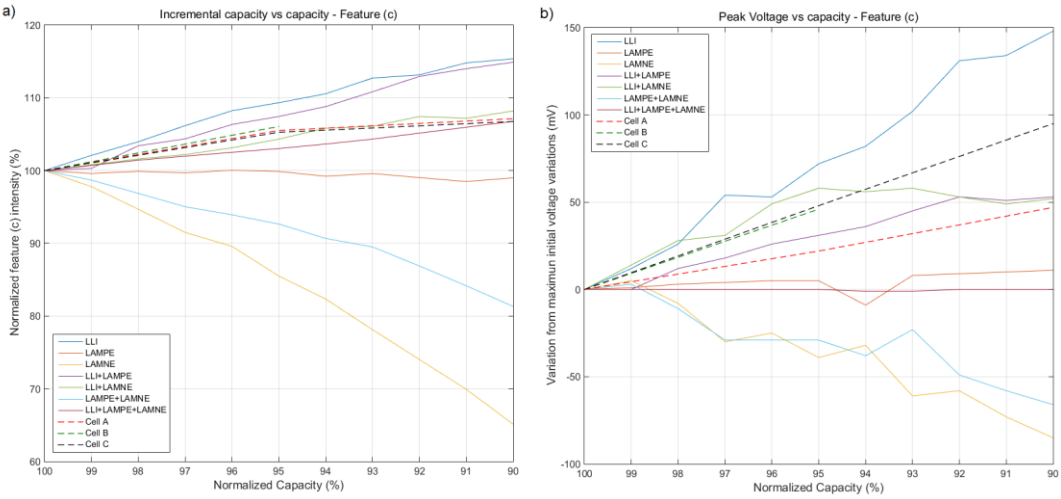

Figure 6: Normalize intensity and peak voltage evolution for feature (c).

4.1.3 Feature (d)

The last feature to consider is the incremental capacity intensity at 4V. Figure 7 shows that the three tested cells share the same evolution with an intensity decrease. According to our comparison with simulated scenarios, the less likely to occur are LAM_{NE}, LLI and LLI+LAM_{NE}.

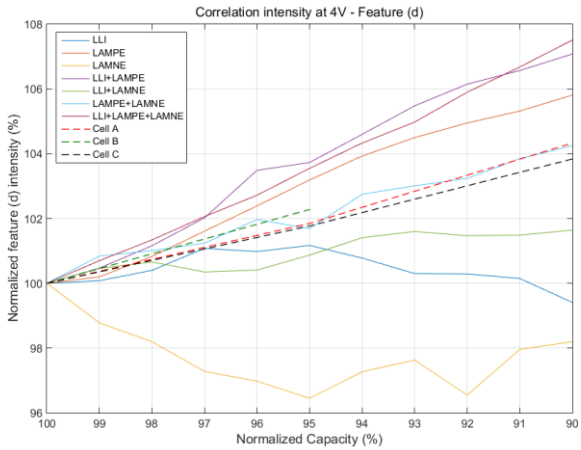

Figure 7: Intensity at 4Vevolution with aging.

4.2 Summary of the observations

In table 1, a summary of the excluded paths is presented. From here, the most likely scenarios list can be compiled.

For this study, 7 scenarios were considered: LLI, LAM_{PE}, LAM_{NE} LLI+LAM_{PE}, LLI+LAM_{NE}, LAM_{PE}+LAM_{NE} and LLI+ LAM_{PE}+LAM_{NE}.

Feature (a) and (b) evolution seems to indicate that LLI and LAM_{NE} are unlikely. Feature (c) evolution allows to exclude LLI, LAM_{NE}, LAM_{PE} and LAM_{PE} +LAM_{NE}.

Finally, feature (d) points towards LLI, LAM_{NE} and LLI+LAM_{NE} being incompatible.

Compiling this information, it seems that most likely scenario for the degradation are LLI+LAM_{PE} and LLI+ LAM_{PE}+LAM_{NE}. However, LAM_{NE} was excluded as a possible degradation mode for all the features, we are therefore considering LLI+LAM_{PE} as the best candidate.

Table 1: Summary of the excluded paths for each feature

Features	Specific parameter	Excluded paths
Feature (a)	Intensity	LLI LAM_{NE} LLI+ LAM_{NE}
	Voltage	LLI LLI+LAM_{NE}
Feature (b)	Intensity	LLI LLI+LAM_{NE}
	Voltage	LLI LLI+LAM_{NE}
Feature (c)	Intensity	LLI LAM_{PE} LAM_{NE}
	Voltage	LLI LAM_{NE} LAM_{PE} +LAM_{NE}
Feature (d)		LLI LAM_{NE} LLI+LAM_{NE}

4.3 Path dependence: Cell A vs. Cell C

As established in the previous section, the most likely degradation path involves LLI+LAM_{PE}. A quantification analysis showed that the trends observed on the experimental data at 90% SoH are best represented with around 5% LLI and 5% LAM_{PE}, figure 8 as it matches the evolution of features (a), (b), (c) and (d)

Overall, this simulation is matching the overall behavior of the 3 cells. Nonetheless, some differences in the aging process, and thus some path dependence of the degradation was observed even though the cells reached the same SoH, 90%. This is especially visible between Cell A that experienced deed discharges (80% DoD) and Cell C that experienced shallow discharges (30%DoD). According to their respective evolution of the features of interest (Section 4.1) and the simulated scenarios (Section 4.2), we can assess that the observed differences between the cells were likely introduced by some additional LAM_{PE} on the cells that performed deep discharges.

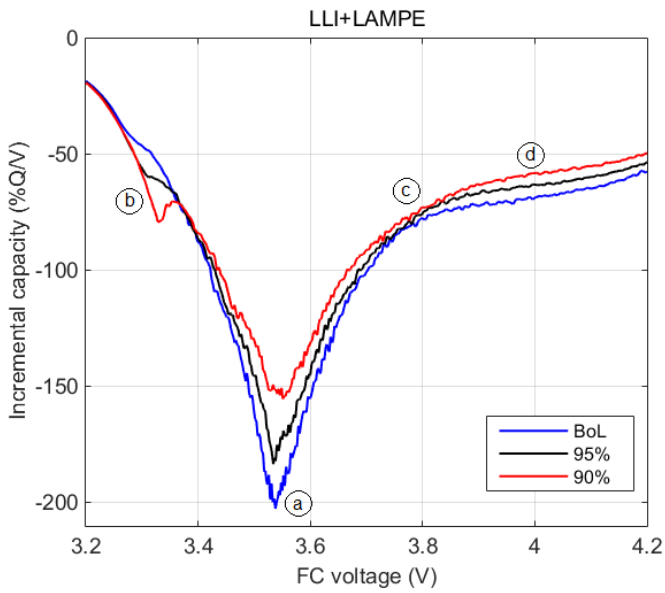

Figure 8: Best fit obtained by mixing LLI and LAM_{PE} by using the *'alawa* toolbox on the left side, and evolution of IC curves obtained from the tested cells in terms of ageing on the right side.

5- Conclusions

The developed work aims to detect and quantify the degradation which is happening in NMC/Graphite cells. Three cells have been tested from a BoL state at different DoDs: 80, 60% and 30%. IC curves have been used for the identification of the possible degradation modes in the 3 cells with the help and use of the *'alawa* toolbox.

From the simulated scenarios in the *'alawa* toolbox and the tested cells comparison, four different characteristics have been detected as the key parameters for degradation mechanisms detection. From these 4 features, a deep comparison between the tested cells and the paths conformed by the different simulated scenarios has been done. All curves have been studied separately in order to compare the degradation with simulated scenarios. A final best fitting curve has been obtained giving as an estimate of the cell degradation mechanisms which involve around 5 % of both LLI and LAM_{PE} after a 10% capacity loss.

Additionally, some path dependence was observed and the cell that performed the shallowest cycling (30%) DoD seems to have experienced less LAM_{PE}.

Acknowledgments

The authors gratefully acknowledge the funding provided by the Etortek program of the Basque Government (Energigune'14 - Desarrollo de actividades de Investigación en Almacenamiento de Energía Electroquímica y Térmica, IE14-388) Strategic Program of the Basque Government.

References

[1] Christophersen JP, Hunt GL, Ho CD, Howell D. Pulse resistance effects due to charging or discharging of high-power lithium-ion cells: A path dependence study. J Power Sources 2007;173:998–1005. doi:10.1016/j.jpowsour.2007.08.025.

[2] Gering KL, Sazhin S V., Jamison DK, Michelbacher CJ, Liaw BY, Dubarry M, et al. Investigation of path dependence in commercial lithium-ion cells chosen for plug-in hybrid vehicle duty cycle protocols. J Power Sources 2011;196:3395–403. doi:10.1016/j.jpowsour.2010.05.058.

[3] Liaw BY, Dubarry M. From driving cycle analysis to understanding battery performance in real-life electric hybrid vehicle operation. J Power Sources 2007;174:76–88. doi:10.1016/j.jpowsour.2007.06.010.

[4] Ma Z, Jiang J, Shi W, Zhang W, Mi CC. Investigation of path dependence in commercial lithium-ion cells for pure electric bus applications: Aging mechanism identification. J Power Sources 2015;274:29–40. doi:10.1016/j.jpowsour.2014.10.006.

[5] Dubarry M, Truchot C, Liaw BY. Synthesize battery degradation modes via a diagnostic and prognostic model. J Power Sources 2012;219:204–16. doi:10.1016/j.jpowsour.2012.07.016.

[6] Han X, Ouyang M, Lu L, Li J, Zheng Y, Li Z. A comparative study of commercial lithium ion battery cycle life in electrical vehicle: Aging mechanism identification. J Power Sources 2014;251:38–54. doi:10.1016/j.jpowsour.2013.11.029.

[7] Bloom I, Christophersen JP, Abraham DP, Gering KL. Differential voltage analyses of high-power lithium-ion cells. J Power Sources 2006;157:537–42. doi:10.1016/j.jpowsour.2005.07.054.

[8] Bloom I, Walker LK, Basco JK, Abraham DP, Christophersen JP, Ho CD. Differential voltage analyses of high-power lithium-ion cells. 4. Cells containing NMC. J Power Sources 2010;195:877–82. doi:10.1016/j.jpowsour.2009.08.019.

[9] Dubarry M, HNEI University of Hawai'i at Mānoa. 'Alawa software. 'Alawa 2015. https://www.soest.hawaii.edu/HNEI/alawa/ (accessed July 14, 2015).

[10] Dubarry M, Truchot C, Cugnet M, Liaw BY, Gering K, Sazhin S, et al. Evaluation of commercial lithium-ion cells based on composite positive electrode for plug-in hybrid electric vehicle applications. Part I: Initial characterizations. J Power Sources 2011;196:10328–35. doi:10.1016/j.jpowsour.2011.08.077.

[11] Dubarry M, Liaw BY. Identify capacity fading mechanism in a commercial LiFePO4 cell. J Power Sources 2009;194:541–9. doi:10.1016/j.jpowsour.2009.05.036.

[12] M. Berecibar, F. Devriendt, M. Dubarry, I.Villarreal, N. Omar, W. Verbeke JVM. Online State of Health estimation on NMC cells based on Predictive Analytics. J Power Sources. - *Submitted*

[13] Kassem M, Bernard J, Revel R, Pélissier S, Duclaud F, Delacourt C. Calendar aging of a graphite/LiFePO4 cell. J Power Sources 2012;208:296–305. doi:10.1016/j.jpowsour.2012.02.068.

[14] Dubarry M, Truchot C, Liaw BY. Cell degradation in commercial LiFePO4 cells with high-power and high-energy designs. J Power Sources 2014;258:408–19. doi:10.1016/j.jpowsour.2014.02.052.

[15] Devie A, Dubarry M, Liaw BY. Overcharge Study in Li4Ti5O12 Based Lithium-Ion Pouch Cell: I. Quantitative Diagnosis of Degradation Modes. J Electrochem Soc 2015;162:A1033–40. doi:10.1149/2.0941506jes.

[16] Dahn HM, Smith AJ, Burns JC, Stevens DA, Dahn JR. User-Friendly Differential Voltage Analysis Freeware for the Analysis of Degradation Mechanisms in Li-Ion Batteries. J Electrochem Soc 2012;159:A1405–9. doi:10.1149/2.013209jes.

[17] Matthieu Dubarry AD and BYL. The Value of Battery Diagnostics and Prognostics. J Energy Power Sources 2014;1:242–9.

[18] Merla Y, Wu B, Yufit V, Brandon NP, Martinez-Botas RF, Offer GJ. Novel application of differential thermal voltammetry as an in-depth state-of-health diagnosis method for lithium-ion batteries. J Power Sources 2016;307:308–19. doi:10.1016/j.jpowsour.2015.12.122.

[19] Birkl CR, McTurk E, Roberts MR, Bruce PG, Howey DA. A Parametric Open Circuit Voltage Model for Lithium Ion Batteries. J Electrochem Soc 2015;162:A2271–80. doi:10.1149/2.0331512jes.

[20] Liu G, Ouyang M, Lu L, Li J, Hua J. A highly accurate predictive-adaptive method for lithium-ion battery remaining discharge energy prediction in electric vehicle applications. Appl Energy 2015;149:297–314.

doi:10.1016/j.apenergy.2015.03.110.

[21] Andrea Marongiu DUS. On-board Aging Estimation using Half-cell Voltage Curves for LiFePO4 Cathode-based Lithium-Ion Battery for Electric Vehicle Application. EVS28, 2015, p. 11.

[22] Ouyang M, Feng X, Han X, Lu L, Li Z, He X. A dynamic capacity degradation model and its applications considering varying load for a large format Li-ion battery. Appl Energy 2016;165:48–59. doi:10.1016/j.apenergy.2015.12.063.

[23] Riviere E, Venet P, Sari A, Meniere F, Bultel Y. LiFePO4 Battery State of Health Online Estimation Using Electric Vehicle Embedded Incremental Capacity Analysis. 2015 IEEE Veh. Power Propuls. Conf., IEEE; 2015, p. 1–6. doi:10.1109/VPPC.2015.7352972.

[24] Dubarry M, Truchot C, Liaw BY, Gering K, Sazhin S, Jamison D, et al. Evaluation of commercial lithium-ion cells based on composite positive electrode for plug-in hybrid electric vehicle applications. Part II. Degradation mechanism under 2C cycle aging. J Power Sources 2011;196:10336–43. doi:10.1016/j.jpowsour.2011.08.078.

Authors

Eng. Maitane Berecibar received her B.S. degree in Electrical and Electronics Engineering from the University of Mondragon, Spain in 2009. She developed her final degree project in the University of Brno, Czech Republic, named “Quality of Service of Free Space Optical Links”. Her M.S. degree in Automatics and Electronics Engineering was obtained in 2012 from University of the Basque Country in Bilbao, Spain. In order to obtain this degree, she developed a project named “Estimating Storage Requirements for Wind Power Plants” at New Jersey Institute of Technology. She is now pursuing her Ph. D. degree between the Technology Research Centre IK4-Ikerlan and the Free University of Brussels, performing the research on “Degradation and estimation algorithms of SoH in Lithium Ion batteries”.

Dr. Eng. Matthieu Dubarry (PhD, Electrochemistry & Solid State Science, University of Nantes), has over 15 years of experience in renewable energy, with an emphasis in the area of lithium ion batteries. Following his master’s degree in ceramic engineering and his PhD on the synthesis and characterization of materials for lithium batteries, Dr. Dubarry joined HNEI to work on the analysis of the usage of a fleet of electric vehicles in 2005. He was later appointed a faculty position in 2010 with a focus on battery testing, modelling and simulation. Matthieu Dubarry major contributions in the battery research are in the area of commercial battery diagnosis and prognosis. He pioneered and is still developing new unique and intuitive methods for non-invasive battery characterization, state of charge and state of health tracking, and simulation of commercial Li-ion batteries and battery packs.

Prof. Dr. Eng. Noshin Omar obtained his M.S. degree in Electronics and Mechanics from Erasmus University College Brussels. He obtained his PhD in 2012 in the department of Electrical Engineering and Energy Technology ETEC, at the Vrije Universiteit Brussel, Belgium. He is the head of the Battery Innovation Center of VUB. Currently he is coordinating several national and European projects in the field of characterisation, electrical, thermal, electrochemical and lifetime modelling of various rechargeable energy storage systems. He was and is still active in various European projects such as SUPERLIB, BATTERIES2020, FIVEVB.

Dr. Igor Villarreal Sarria received his PhD in Electrochemistry in 2001 from the CSIC-UCM. He joined IK4-IKERLAN in 2001 and spent 2 years in Lawrence Berkeley National Laboratory working in SOFC. Since 2010 he is the team manager of Energy Storage Systems group and since 2015 the main responsible of Energy Storage and

Management research area at IK4-IKERLAN. He has directed several PhD students and has many publications on electrochemistry.

Prof. Dr. Eng. Joeri Van Mierlo leads the MOBI – Mobility, Logistics and automotive technology research centre (http://mobi.vub.ac.be). A multidisciplinary and growing team of 60 staff members. Prof. Van Mierlo was visiting professor at Chalmers University of Technology, Sweden (2012). He is expert in the field of Electric and Hybrid vehicles (batteries, power converters, energy management simulations) as well as to the environmental and economical comparison of vehicles with different drive trains and fuels (LCA, TCO).